44th AIAA Plasmadynamics and Lasers Conference
26-29 June 2013, San Diego, CA
AIAA-2013-3136

The Estimation of the Unsteady Aerodynamic Force Applied to a Turret in Flight

Nicholas De Lucca[1], Stanislav Gordeyev[2], Eric Jumper[3]
University of Notre Dame, Notre Dame, Indiana 46545, USA

Kyle Hird[4], Thomas J. Juliano[5], James W. Gregory[6]
The Ohio State University, Columbus, Ohio 43235, USA

James Thordahl[7] and Donald J. Wittich[8]
Air Force Research Laboratory, Directed Energy Directorate, Kirtland AFB, NM 87117

The spatially-temporally-resolved pressure field on a surface of a hemisphere-on-cylinder optical turret was characterized in a wind tunnel at M = 0.33 using fast-response Pressure Sensitive Paint (PSP), simultaneously with 8 pressure sensors. A sparse unsteady pressure field was also obtained in-flight for subsonic speeds of M = 0.5 on the Airborne Aero-Optical Laboratory (AAOL) using 26 unsteady pressure sensors. Using the unsteady pressure data from PSP tests, the unsteady forces acting on the turret in the tunnel were calculated and discussed for different turret geometries and window viewing angles. Unsteady forces and moments acting on the turret in-flight were estimated using Linear Stochastic Estimation for different turret geometries and speeds and compared to the tunnel results. Using Proper Orthogonal Decomposition dominant surface pressure modes responsible for unsteady forces were identified and discussed.

1. Introduction

The hemisphere-on-cylinder turret is often used for airborne optical systems to maximize the potential field-of-regard. The turret geometry has been previously shown to feature a highly three-dimensional turbulent flow field [1]. This three-dimensional turbulent flow field has the effect of limiting the effective field-of-regard of the turret, as turbulent regions of compressible flow introduce aberrations in the incident laser beam. The aero-optical environment of a hemisphere-on-cylinder turret has been studied extensively in recent years [1]. There has been a large parametric study of the aero-optical properties of this geometry in-flight for subsonic and transonic speeds using the Airborne Aero-Optics Laboratory, AAOL [2,3]. Additionally a variety of CFD studies have been performed on various turret geometries [4,5,6]. Finally, several flow control strategies have been studied on this turret geometry to improve aero-optical effects [5,7].

As the turret is not a rigid body, typically constructed as a thin-shell body with various optical and mechanical components inside, the turret motion can introduce various mechanical vibrations into optical components and, consequently, into a laser beam projected from it. From a practical perspective, a jitter imposed on the outgoing laser beam of only a few microradians can result in the beam missing a distant target. One source of the unsteady force acting on the turret is the aircraft mechanical vibrations. The second component of the unsteady force arises from

[1] Graduate Student, Department of Aerospace and Mechanical Engineering, Hessert Laboratory for Aerospace Research, AIAA Student Member.
[2] Research Associate Professor, Department of Aerospace and Mechanical Engineering, Hessert Laboratory for Aerospace Research, AIAA Associate Fellow.
[3] Professor, Department of Mechanical and Aerospace Engineering, Hessert Laboratory for Aerospace Research, Notre Dame, IN 46556, AIAA Fellow.
[4] Undergraduate Research Assistant, Department of Mechanical and Aerospace Engineering, 2300 West Case Rd.
[5] Postdoctoral Research Associate, Department of Mechanical and Aerospace Engineering, 2300 West Case Rd., AIAA Member. Currently NRC Postdoctoral Research Fellow at Air Force Research Laboratory, Wright-Patterson AFB, OH.
[6] Assistant Professor, Department of Mechanical and Aerospace Engineering, 2300 West Case Rd., AIAA Senior Member.
[7] Sr. Project Engineer, The Aerospace Corporation, 2155 Louisiana Blvd, Suite 5000, Albuquerque, NM 87110
[8] Aerospace Engineer, Laser Division, 3550 Aberdeen Ave SE

unsteady pressure fluctuations that are due to the turbulent flow features around the turret, and the integrated effect of these fluctuations is an unsteady aerodynamic forcing of the surface of the turret. This jitter is termed the aero-mechanical jitter of the turret. This is not the only jitter that is imposed on the beam, as aero-optical structures present in the turbulent flow over the aperture can also deflect the laser beam directly, so-called aero-optical jitter [1]; prior work has shown the correlation of the aero-mechanical jitter of a laser with the aero-optical jitter [9].

This paper presents the analysis of the unsteady force measurements acting on the turret using results from two experiments. The first experiment used Pressure Sensitive Paint (PSP) to measure the spatially-temporally-resolved pressure fields on the surface of the turret with different realistic geometric features at several viewing angles in a subsonic tunnel, simultaneously with unsteady pressure at several points using unsteady pressure sensors, mounted on the turret. The second test used the same turret to collect unsteady pressure data, using a larger, but still sparse array of unsteady pressure sensors, in-flight at higher subsonic speeds using AAOL.

2. Experimental Setup

I. PSP experiment

The tested turret model, one foot in diameter and 10.4 inches in height, was an exact replica of AAOL turret shell, shown in Figure 1, used for aero-optical flight tests [10]. The turret had a rotating portion, allowing to change the elevation angle and the whole turret assemble can be rotated to any azimuthal angle. The turret had several realistic features, like small gaps between the rotating portion of the turret and trunnions, as well as cut-outs, or "smiles", on both sides of the stationary portion of the turret, typically used to increase field-of-regard at low elevation angles.

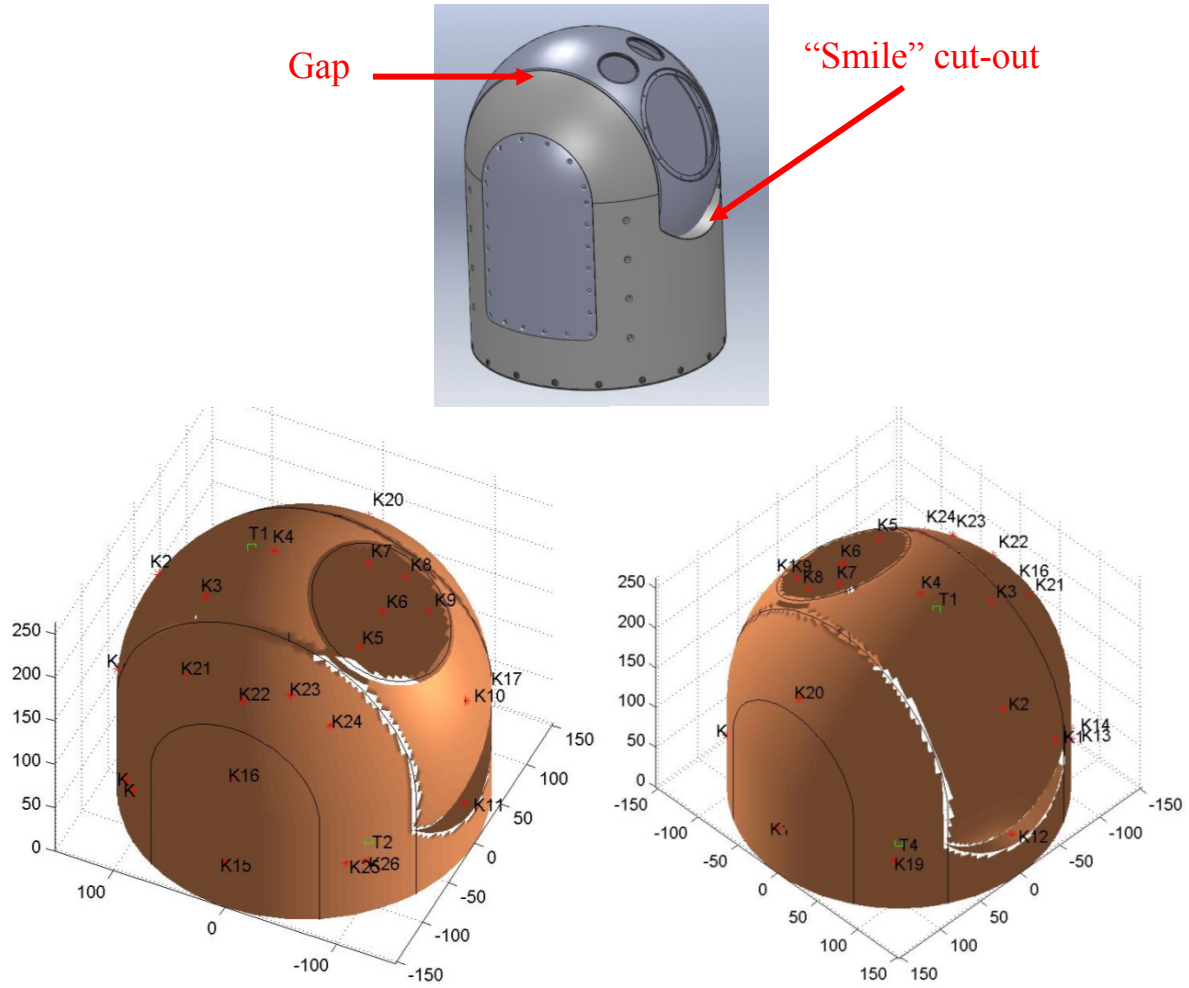

Figure 1. Top: Turret Model. Bottom: Locations of pressure sensors K1-K26 and thermoprobes, T1-T5.

A complete description of the PSP tests is presented in [11], so only essential details will be provided in this paper. The polymer-ceramic/PtTFPP paint with a frequency response up to at least 6 kHz was used [12]. The pressure sensitive paint measurements were acquired in the White Field wind tunnel at the University of Notre Dame, see Figure 2. The wind tunnel is a closed-return tunnel and capable of up to Mach 0.6. In this test, data were acquired at M = 0.33. The turret assembly allowed a continuous variation in both azimuthal and elevation angles. Additionally, the turret aperture window can be switched between a flat window and a conformal one. Figure 3 presents a picture and a schematic of the layout of the experimental hardware. Three different cameras, two on both sides on the test section and one on the top, were used to capture the pressure field, to allow for full surface pressure mapping of the turret. The three cameras acquired images at 2000 Hz for 2.75 seconds. Relevant details about each camera are given in Table 1. Additionally, eight unsteady pressure sensors, 10-psi differential Kulites, K2, K6, K11, K12, K15 K18, K20 and K22, shown in Figure 1, were used to verify the time-variation of the PSP data and provide a reference pressure for analysis. The pressure sensors were referenced to the interior pressure of the turret, which was measured with an external system. To complement the pressure sensors, five thermocouples were placed on the surface of the turret, see Figure 1, bottom row, to account for any temperature variation between tunnel on/off conditions or any temperature gradients across the turret; however, the thermocouple data will not be presented directly in this paper. The unsteady pressure and thermocouple data were acquired at 100 kHz for 10 seconds. The pressure-temperature data acquisition system was triggered simultaneously with the cameras, and digital images were acquired by all cameras simultaneously with the pressure and thermocouple data. Data were taken for several window viewing angles, given in Table 2.

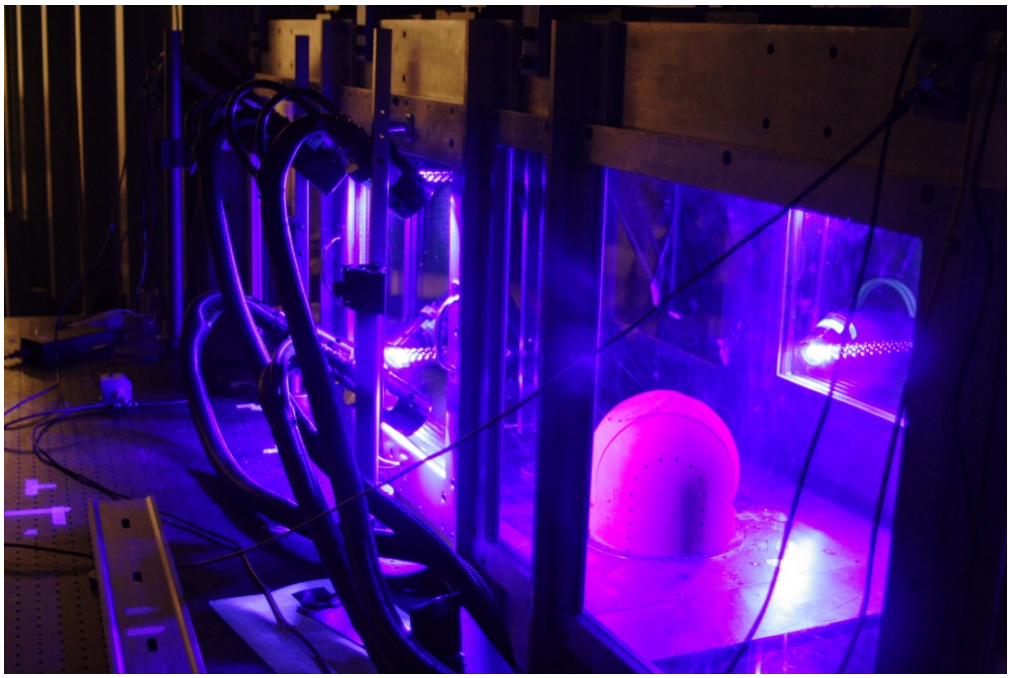

Figure 2. Turret model in the test facility.

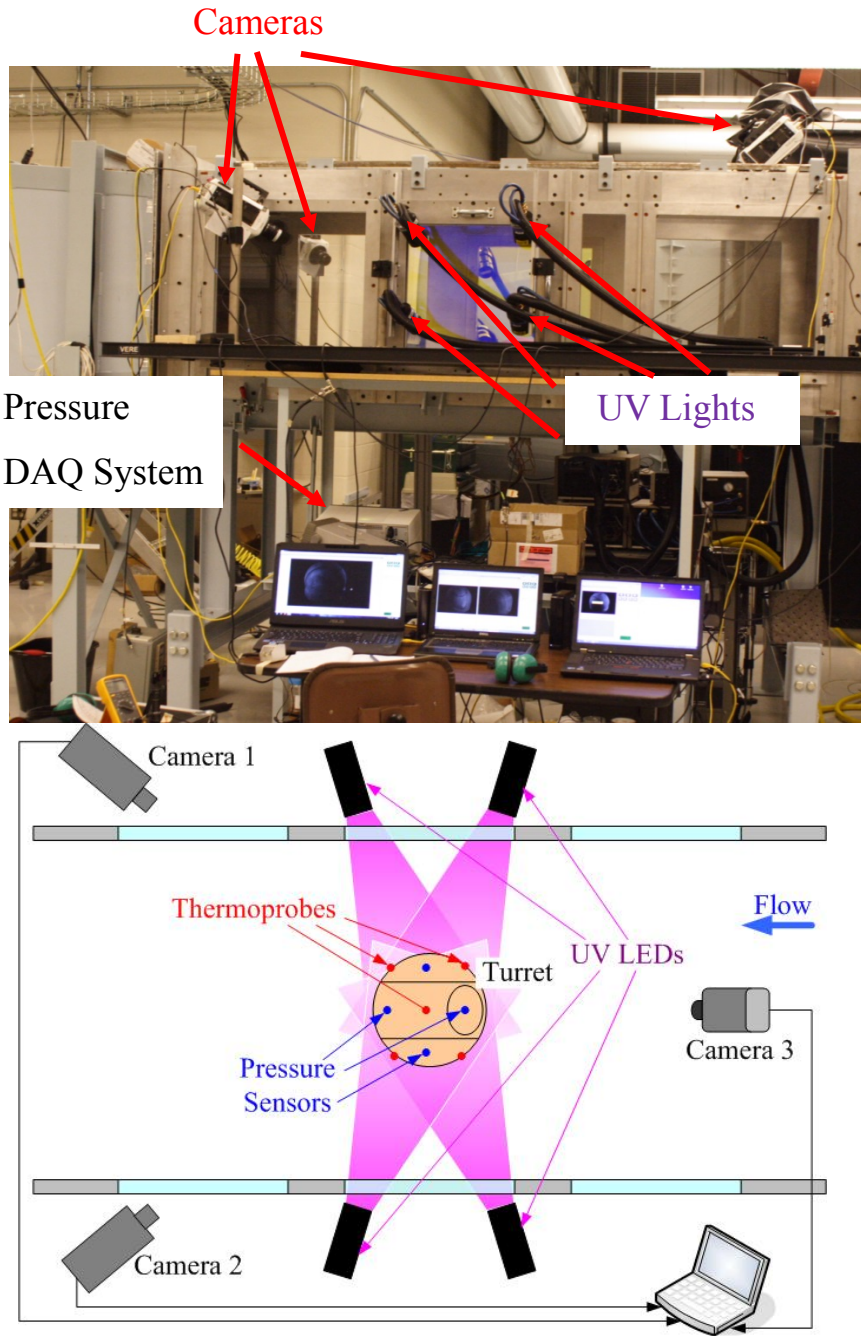

Figure 3. Hardware configuration: Picture (top) and schematic from the top view of wind tunnel. (bottom).

Table 1. Camera properties.

	Camera 1	Camera 2	Camera 3
Colorspace	Greyscale	Greyscale	RGB
Resolution	1280 × 800	1024 × 768	1280 × 800
Frame Limit	5,477	7,000	7,000
Frames per Second	2,000	2,000	2,000

Table 2. Test matrix of turret positions.

		Azimuth				
		0°	90°	125°	143°	180°
Elevation	45°	×	×			×
	60°				×	
	65°		×			
	69°			×		

II. Flight experiment

To collect in-flight pressure data, the same turret was instrumented with additional pressure sensors, bringing the total amount of sensors to 26, see Figure 1, bottom plots; however Kulites 8,12,15, 18 and 25 were found to give erratic flight data so that only a total of 21 pressure sensors gave reliable data. The turret was mounted out of a modified escape hatch in a Cessna Citation Bravo in a full-turret configuration [2, 10]; see Figure 4 for a picture of the turret mounted in the aircraft. The thermocouple data was also acquired in-flight. The flight conditions were M = 0.4 or M = 0.5 at 15000 ft. and M = 0.65 at 29000 ft. In-flight, the elevation and azimuthal angles were manually set via a worm gear and a chain with a hand crank, respectively, shown in Figure 4, bottom, to match viewing angles during the PSP tests, given in table 2. The turret was tested with both the flat and the conformal window. Pressure data were acquired for 30 seconds at 25 kHz. Temperature data were collected at 10 Hz, along with total and static pressures from a Pitot probe installed approximately one turret diameter below the turret.

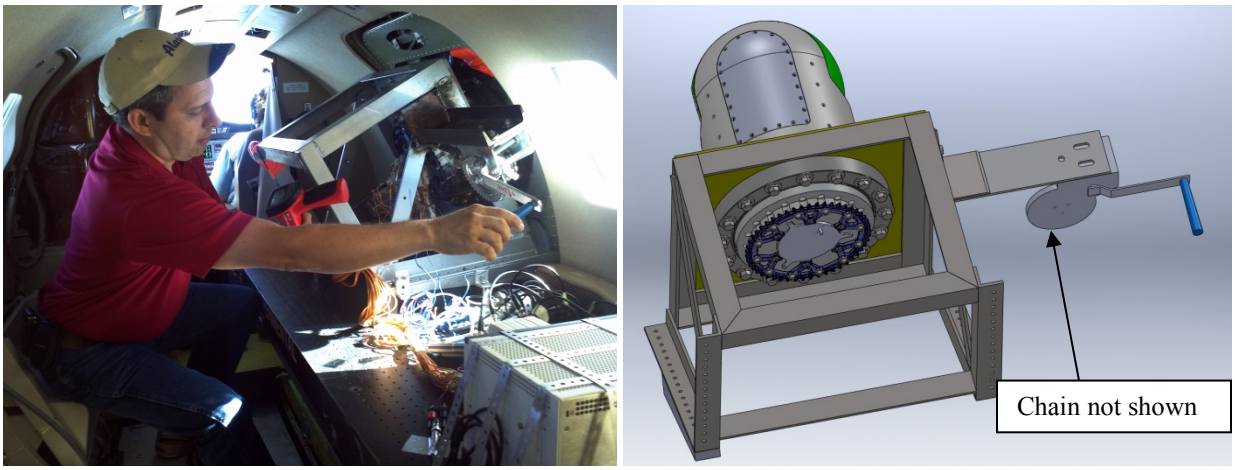

Figure 4. Turret with a conformal-window mounted on the AAOL (top) and the turret viewing-angle control setup, picture (bottom left) and a drawing (bottom right).

3. Data Reduction

III. PSP calibration

A calibration was performed using a painted coupon placed in a pressure- and temperature-controlled calibration chamber. At each of a specified series of conditions, an image of the coupon was made, and the conditions and average intensity recorded. Reference conditions were chosen to closely approximate those of the wind-off runs, and the pressure and intensity were normalized by these reference conditions. Surface fitting was employed to provide a function returning pressure ratio as a function of intensity ratio and instantaneous temperature.

This calibration was employed to deduce instantaneous pressure from the registered images. The elementwise ratio of the wind-off mean to each wind-on frame was calculated, providing for each pixel a value of I_{ref}/I. Early testing explored the possibility of using the average of the registered wind-on frames as the reference condition, but it was found that the change in temperature made this unsuitable for a reference condition. The advantage of using the wind-on reference as a reference is that bulk pressure shifts are cancelled out, isolating the temporal variations. To obtain this effect while maintaining the best fidelity to the data, a two-step procedure was implemented, where the wind-on mean was referenced directly to the wind-off mean, providing a base pressure ratio, i.e. $P_{ref_{on}}/P_{ref_{off}}$. The quotient of the instantaneous pressure ratio and the average pressure ratio provides a more accurate value of $P/P_{ref_{on}}$. A complete description of the calibration procedure is given in [11].

IV. Pressure reconstruction from PSP tests

Knowing exact location of each camera, relative to the turret, it is possible to map the pressure variation from 2-D images onto the 3-D surface of the turret, using Perspective Transformation Matrix technique [13]. The turret surface was split into three regions to provide a unique mapping between the turret surface and the corresponding cameras' images. Using PTM, pressure values on the surface of the turret in each region were computed and, using weighing functions, the full 3-D pressure filed was reconstructed, see [11] or [14] for details. An example of 3-D reconstruction is shown in Figure 5, where individual 2-D pressure fields from images, shown in the top row, were projected onto the 3-D turret surface, shown in the bottom row. Thus, results from all three cameras can be used to reconstruct the spatially-temporally-resolved pressure field over the entire turret surface. For this testing, however, there were noise and intensity issues that resulted from Camera 3 being a color camera [11]. As a result, all further analysis was done using only Cameras 1 and 2. Note that all the presented analysis can be directly expanded to using all three cameras.

4. Results

To determine the unsteady force applied to a turret, the full three dimensional pressure field must be known at each time step. The force is obtained by integrating the pressure over the entire turret, $\vec{F} = \int P\vec{n}dA$, where $\vec{n}$ is an outward unit surface vector; however, in-flight, measurements of the full pressure field are very costly at best. A more practical and efficient way to determine the force is to approximate it from a series of point measurements around the turret. As will be presented later, the integrated force obtained from the PSP data in the tunnel can be correlated with data from a sparse array of unsteady pressure sensors using the Linear Stochastic Estimation (LSE) technique [15]. This technique uses the correlation tensor between a quantity to be estimated and other measured quantities. It can be written as $\tilde{x}_i = L_{ij}y_j$, where $L_{ij} = \langle x_i y_k \rangle \langle y_j y_k \rangle^{-1}$. The signal x_i is to be approximated using a linear sum of other quantities, y_i, that are multiplied by a matrix derived from the cross-correlation tensor, L_{ij}. This is a purely statistical technique; it needs no assumptions about relationships between the quantities. An example of using LSE technique to separate aero-optical and aero-mechanical jitter is given in [9].

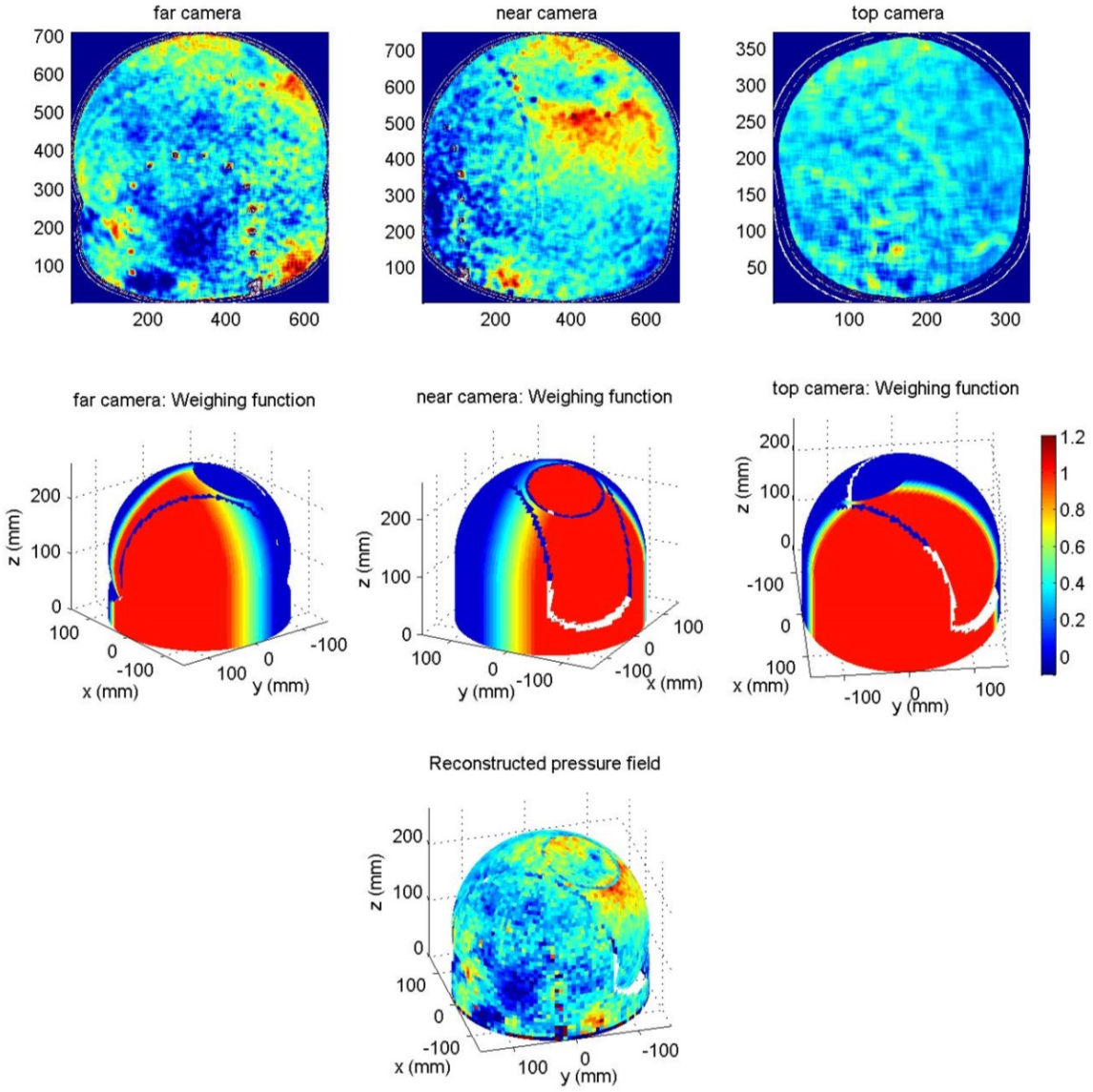

Figure 5. Top: Individual Frames from cameras. Middle: corresponding weighting functions. Bottom: reconstructed instantaneous pressure field on the surface of the turret. Flow goes along x-axis from positive to negative values.

In this paper a spectral version of the LSE-technique is used. The unsteady force spectrum is estimated from the array of pressure sensors, $\{p_i\}$, as,

$$\hat{F}_j^{LSE}(St) = \sum_i C_i^j(St)\hat{p}_i(St),$$

where $C_i^j(St) = \dfrac{\left\langle \hat{F}_j^*(St)\hat{p}_i(St)\right\rangle}{\left\langle \hat{p}_i^*(St)\hat{p}_i(St)\right\rangle}$ is the response matrix computed from PSP tests. Here *St* is the Strouhal number, used to non-dimensionalize the frequency by flow parameters, $St = fD/U$, f is the frequency, D is the turret diameter, and U is the freestream flow velocity. Additionally, as the unsteady pressures obtained in-flight and in the tunnel are taken at different flow conditions, pressures were normalized by the dynamic pressure, q, defined as $q = \frac{1}{2}\rho U^2$, with ρ being the freestream density. The x-direction is the streamwise direction, with positive x pointing upstream, corresponding to Az = 0°. The y-direction is the cross-stream direction, corresponding to an

azimuthal angle of 90°. The z-direction is the vertical direction, pointing away from the mounting wall, along the elevation angle of 90°.

Finally, it is also useful to non-dimensionalize the integrated force by the product of the dynamic pressure and cross-sectional area of the turret, $S = 1/8\,\pi D^2 + DH$, with H = 4.35" being the height of the cylindrical base. The power spectrum of the non-dimensional force will be determined using a linear combination of the non-dimensional pressure spectra, and the result can then be re-dimensionalized to the desired flight conditions.

I. PSP Verification

The first step in producing accurate force estimates is verifying the accuracy of the PSP data. As the force spectrum will be reconstructed using a linear combination of pressure spectra from pressure sensors, the pressure spectra collected both in the tunnel and in-flight must be similar. Additionally, the pressure spectra obtained from PSP experiments must match that obtained from the Kulites in the tunnel, to verify the accuracy of the PSP data. Figure 6 shows the non-dimensional pressure power spectra for one of the Kulites at two different viewing angles for both in-flight and tunnel cases. The extracted local pressure spectra obtained from the PSP at the same locations are shown as well. The non-dimensional spectra were obtained by dividing the normalized pressure by the sample rate and Fourier Transform block size. As the plot shows, there is very good agreement in both magnitude and frequency content between the normalized pressure spectra collected in the tunnel from the Kulite and the PSP, except for the very end of the PSP-spectrum, where PSP spectra have a small energy build-up due to insufficient sampling rate. There is also good agreement between the pressures obtained in the tunnel and those in-flight at Az = 126° and 180°, Figure 6, middle and right plots. For Az = 90°, Figure 6, left plot, the general shape is still obtained, but there is a noticeable peak in the tunnel data, for both Kulite and PSP, at St = 0.15. This will be discussed in details later. Additionally, this agreement only holds for subsonic flows; if the flow becomes transonic or supersonic, the flow topology undergoes a significant change [1,2] that will not be accounted for in the response matrix.

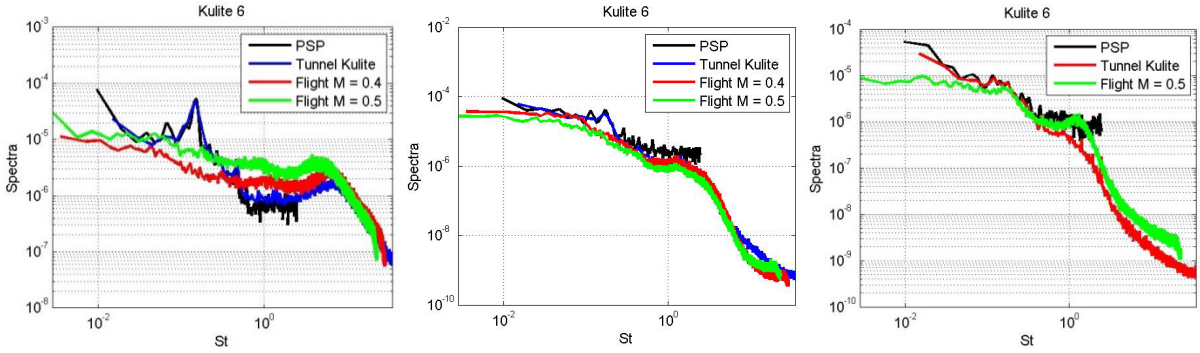

Figure 6. Spectra comparison between flight and PSP. (Left) Az = 90, El = 65, (middle) Az = 126, El = 69, (right) Az = 180, El = 45. All cases were collected for the turret with the flat window.

II. POD and Force Analysis

To better understand the relation between the instantaneous pressure field, $p(s,t)$, where s is the point of the turret, and the global forces, resulting from it, it is useful to decompose the pressure field into a liner combination of orthogonal pressure modes, using a Proper Orthogonal Decomposition (POD) technique [16], as

$$p(s,t) = \sum_n a_n(t)\varphi_n(s), \tag{1}$$

$$\text{where } a_n(t) = \int_S p(s,t)\varphi_n(s)ds, \quad \overline{a_n(t)a_m(t)} = \lambda_n \delta_{nm}$$

and spatial POD modes, $\phi_n(s)$, and corresponding eigenvalues or mode energies, λ_n, are solution of an integral equation,

$$\int_S R(s,s')\varphi_n(s')ds' = \lambda_n \varphi_n(s), \quad R(s,s') = \overline{p(s,t)p(s',t)}$$

The detailed analysis of POD pressure modes and their dependence of the turret geometry and window viewing angle is given in [14], so here we will only discuss the relation between POD pressure modes and unsteady forces.

Time-dependent force components, $F_i(t)$, can be found by integrating Eq. (1) over the surface of the turret,

$$F_i(t) = \sum_n a_n(t) \int_S \varphi_n(s) n_i(s) ds = \sum_n a_n(t) b_i^n, \quad b_i^n = \int_S \varphi_n(s) n_i(s) ds,$$

where $\{n_i(s)\}$ is a unit outward vector, normal to the surface of the turret. So, the force is linearly proportional to the temporal evolution of the POD pressure modes, weighed by the influence coefficients, b_i^n, which are function of the geometry and viewing angles. Consequently, the time-averaged square-value of the force, or the force "energy", $F_{i,rms}^2$, can be found as,

$$F_{i,rms}^2 = \sum_n \lambda_n \left(b_i^n\right)^2 = \sum_n F_i^n$$

where F_i^n are analogous to eigenvalues of the POD pressure modes and describe the contribution of the n-th POD pressure mode to the i-th component of the force. Similarly, the cumulative eigenvalue, $\Omega_i^n = \sum_m^n F_i^m / \sum_m F_i^m$, can be introduced to describe the contribution of the first n POD pressure modes to the overall level of $F_{i,rms}^2$.

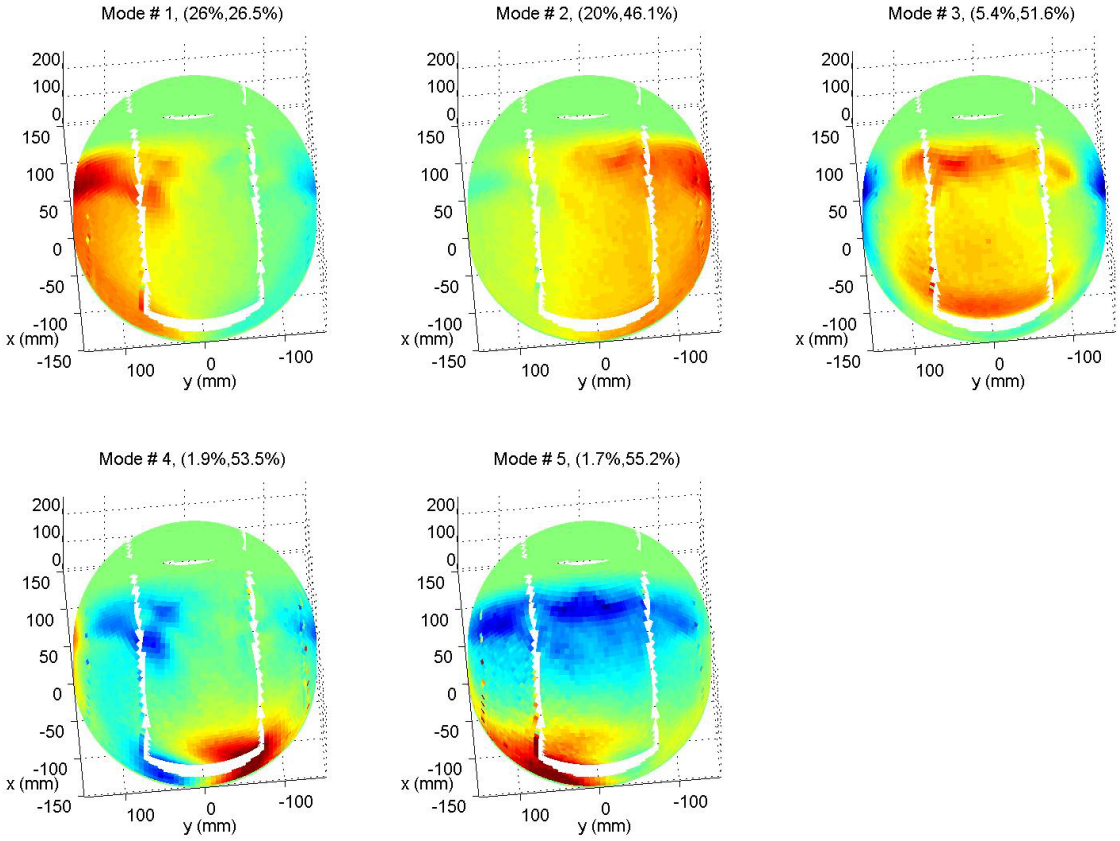

Figure 7. First 5 POD modes for Az = 0 degrees, El = 45 degrees for the conformal-window turret. The corresponding normalized and the cumulative energies for each POD mode are given as a first and a second numbers in parenthesis on top of every plot. The flow goes along x-axis from positive to negative values.

Example of the first five POD pressure modes for Az = 0 degrees and El = 45 degrees for the conformal-window turret are presented in Figure 7. The first two POD modes have 26% and 20% of the total pressure energy and the spatial distributions of these modes reveal that they correspond to the separation-line-related pressure fluctuations. Thus, the separation-related pressure fluctuations are dominant source of the overall pressure fluctuations on the

surface of the turret. These two modes appear to be almost mirror images of each other relative to the vertical streamwise centerplane and have essentially non-zero values only at one side of the turret; as POD modes are statistically-uncorrelated, this suggests that the separation-related pressure fluctuations on both sides of the turret are also statistically-independent. The third mode is also related to the separation line, but mostly on top of the turret; it appears to be symmetric relative to the vertical streamwise centerplane. Modes 4 and 5 are related to the unsteady stagnation region at the bottom of the turret, caused by the recirculating flow downstream of the turret. Overall, first five dominant modes contain 55% of the fluctuating pressure energy.

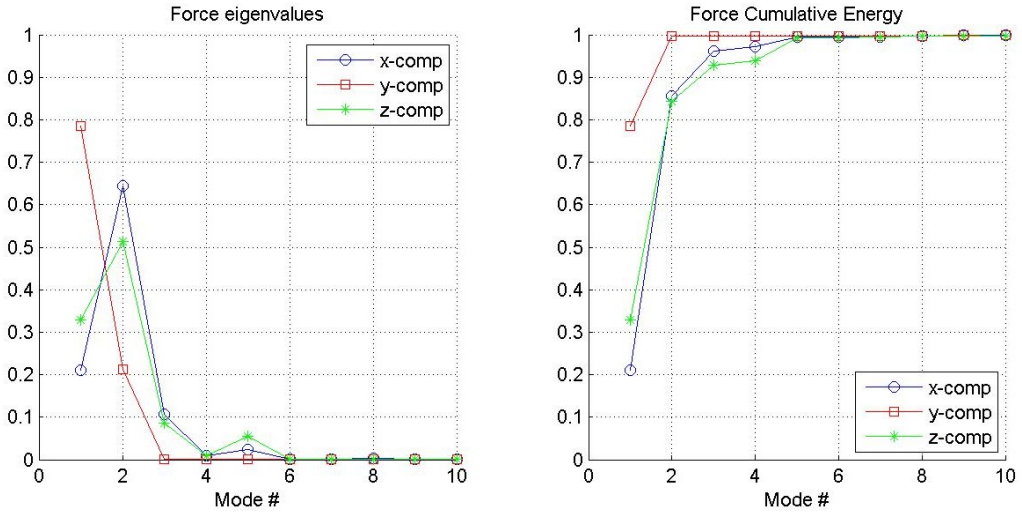

Figure 8. Force normalized eigenvalues, $F_i^n / \sum_n F_i^n$, (left) and cumulative eigenvalues, Ω_i^n , (right) for the conformal-window turret, Az = 0 degrees, El = 45 degrees.

Force normalized eigenvalues, $F_i^n / \sum_n F_i^n$, and cumulative eigenvalues, Ω_i^n , for the conformal-window turret, Az = 0 degrees and El = 45 degrees are presented in Figure 8. From here it follows that it takes only first 5 pressure modes to completely describe the temporal evolution of the force components; also, each pressure mode has a different contribution of the unsteady force. As the force is a surface integral of the pressure field, local pressure features might cancel each other during the integration. Thus, while a pressure mode might be important to describe unsteady pressure field, its influence coefficient might be small for a given force component. For instance, the y-component of the force depends only on the first two pressure modes, while 4th pressure mode does not contribute to any of the force component, see Figure 8.

When the turret was rotated to Az = 90 degrees, both smiles were positioned symmetrically on both sides of the turret, relative to the incoming flow. It was shown in [14] that the prematurely-forced flow separations are caused by the "smile" slope discontinuities and are responsible for a significant increase of the pressure fluctuations downstream of "smiles"; thus, dominant POD modes for Az = 90 degrees and El = 45 degrees, conformal-window case, shown in Figure 9 are significantly different from the corresponding POD modes for the conformal-window turret for Az = 0 degrees and El = 45 degrees, shown in Figure 7. The spatial distribution of the first mode is spanwise anti-symmetric at this angle, suggesting that the separation-related pressure fluctuations on both sides of the turret are strongly correlated and out-of-phase; recall that separation-related modes 1 and 2 for Az = 0 degrees and El = 45 degrees were largely uncorrelated. POD modes 3-5 are related to the unsteady stagnation region on the bottom of the turret.

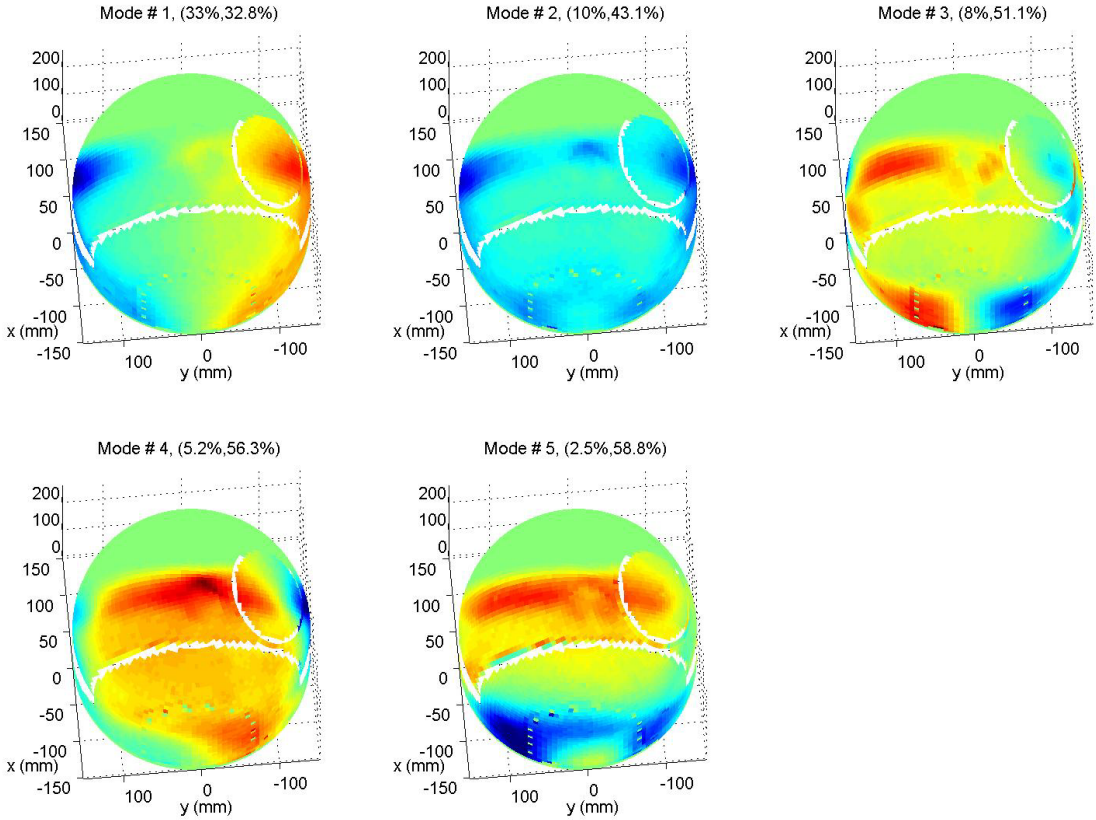

Figure 9. First 5 POD modes for Az = 90 degrees, El = 45 degrees for the conformal-window turret. The corresponding normalized and the cumulative energies for each POD mode are given as a first and a second numbers in parenthesis on top of every plot. The flow goes along x-axis from positive to negative values.

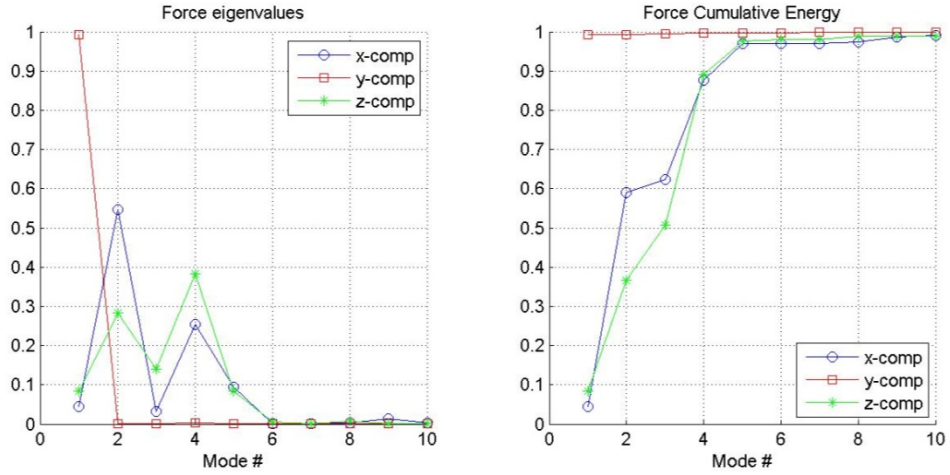

Figure 10. Force normalized eigenvalues, $F_i^n / \sum_n F_i^n$, (left) and cumulative eigenvalues, Ω_i^n , (right) for the conformal-window turret, Az = 90 degrees, El = 45 degrees.

Force normalized eigenvalues, $F_i^n / \sum_n F_i^n$, and cumulative eigenvalues, Ω_i^n , for the conformal-window turret, AZ = 90 degrees and EL = 45 degrees are presented in Figure 10. From here it follows that it takes only first 5 pressure modes to completely describe the temporal evolution of the force components; also, each pressure mode

has a different contribution of the unsteady force. At this viewing angle, the y-component of the force depends only on the first pressure mode, and the first five modes are sufficient to describe all essential temporal behavior of the unsteady force. Analysis of all cases (not shown) showed that dynamics of the first five POD pressure modes are enough to correctly describe the temporal evolution of the unsteady force components for all tested geometries and window viewing angles.

An example of power spectra of the temporal coefficients of the dominant five modes for the conformal-turret for Az = 0 degrees and El = 45 degrees are presented in Figure 11. First two modes have a peak around $St_D = 0.15$ and a smaller and sharper peak around $St_D = 0.5$. As will be discussed in the following sections, these first two modes are primary drivers of the cross-stream unsteady force applied to the turret.

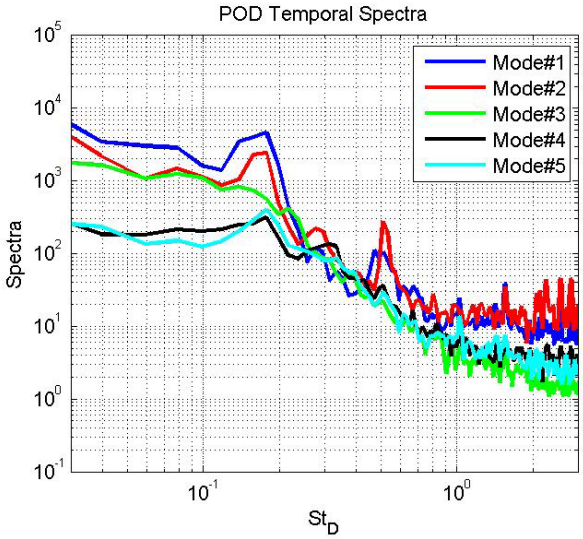

Figure 11. Spectra for temporal coefficients for first 5 POD modes for Az = 0 degrees, El = 45 degrees for the conformal-window turret.

III. Force Reconstruction

The spectra of the unsteady force computed from the continuous pressure field from PSP tests, as well as reconstructed with the LSE technique using progressively-sparser arrays of the pressure sensors are presented in Figure 12 for the flat-window turret with Az = 126 degrees and El = 69 degrees. In addition, the unsteady force estimates from in-flight measurements are also presented in Figure 12. The solid black line shows the actual computed non-dimensional force from the PSP data. The blue and red lines show the approximation of the force reconstructed using the local pressure spectra obtained from the PSP measurements; the blue line corresponds to the reconstructed force if all 26 Kulites were working properly while the red line uses only 21 Kulites that were verified to be working properly in-flight. Finally, the green line gives the force reconstructed using data obtained in-flight at M = 0.5. The first conclusion is that the force from the tunnel experiments is exceptionally-well reconstructed using several local pressure measurements. The blue and red lines begin to fall slightly below the actual compute force for St > 0.6. The reason for this lies in the sparse sampling of the pressure field. Relevant turbulent structures that contribute to the unsteady forcing have different spatial extent, while the reconstruction uses information from a series of point pressure measurements. The smaller the structure the more sensors it requires to be resolved. So, all the relevant turbulent structures may not be captured with the local pressure measurements.

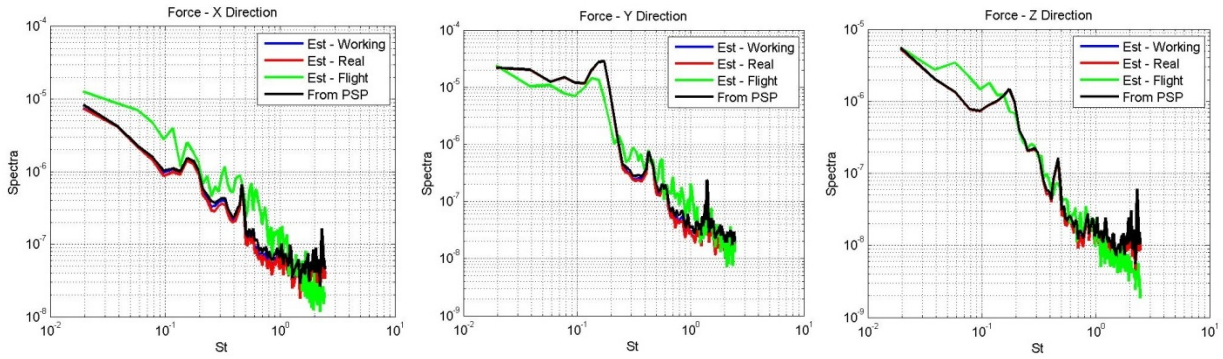

Figure 12. The spectra of the LSE-reconstruction of all components of the unsteady force using different number of in-flight pressure sensors compared with the integrated value from PSP tests. The turret geometry was the conformal-window turret with Az = 126° and the El = 69°.

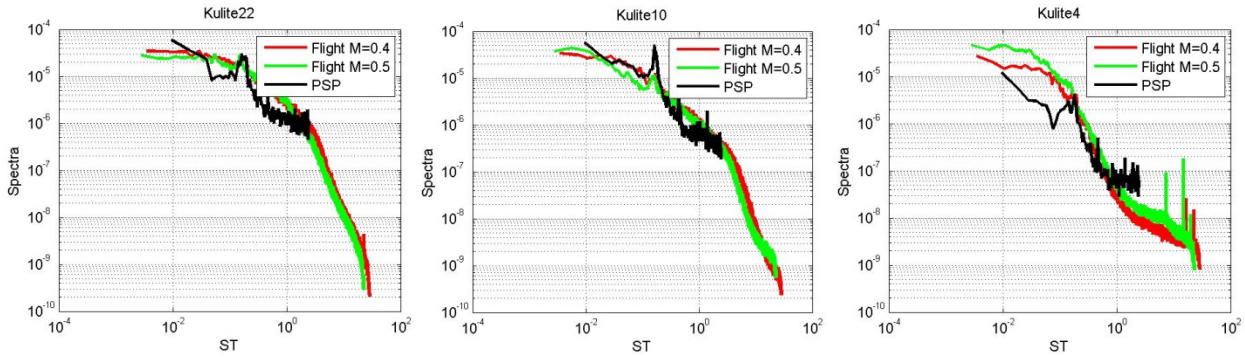

Figure 13. PSP and Kulite spectra for three kulites at Az = 126°, El = 69° with a conformal window.

The force estimated from in-flight sparse unsteady pressure data shows good overall agreement with the estimate from the tunnel pressure measurements, with a few distinct differences. First, the x-direction force, an unsteady drag, is larger in-flight across a range of Strouhal numbers. To investigate this, let us examine unsteady pressure spectra in selected locations. These spectra are given in Figure 13. The Kulite in Figure 13, left plot, labeled K22 in Figure 1, is in a location where the normal vector points mostly along the x-direction. For this location, the in-flight pressure is also almost universally larger, except in the $0.15 < St < 0.2$ range, as observed in Figure 8, left plot. The y-force, an unsteady spanwise force, shows a similar trend when compared with a sensor K10, located where the normal surface vector corresponds mostly to the y-direction at this viewing angle. Compared with the M = 0.5 flight data, the pressure spectrum in the tunnel is larger until St = 0.2, the same spectral behavior observed for the y-direction force spectrum, see Figure 7, middle plot. As with the x- and y-components, the z-component, the unsteady lift, shows the exact same behavior when compared with an unsteady pressure sensor K4, located on top of the turret. The estimated z-force spectrum tends to be larger in-flight in the same St ranges that the measured unsteady pressure spectrum. This is the expected result, since the estimated force spectra are linear weighted summations of the unsteady pressure spectra for each component. For large St, the force spectra calculated directly from the PSP measurements shows the same energy build-up that was observed in the pressure spectra. As mentioned before, this energy build-up is due to an insufficient sampling rate for the PSP measurements. In the POD section, it was shown that only five orthogonal pressure modes are needed to fully prescribe the force applied to the turret. The LSE technique essentially correlates the sum of those integrated modes with select point measurements, as the force contribution of the remaining modes is negligible. Thus, as long as the five dominant pressure modes do not substantially change between flight and tunnel testing, the LSE technique will accurately approximate the force applied to the turret. A further discussion and possible explanation of some of the differences observed between the tunnel and flight testing will be presented later in the paper.

IV. Force analysis for different Azimuth and Elelvation

Figure 14 gives the forces' spectra calculated directly from the PSP measurements for all the measured viewing angles. The first trend is that the window geometry has a very limited effect on the force applied to the whole turret. This behavior may seem unexpected; however, it should be kept in mind that the window surface area is small

compared to the total surface area of the turret. Additionally, though changing from the conformal to the flat window has the effect of tripping the flow and changing the unsteady pressure distribution over the window for some viewing angles, this effect is less in magnitude compared to a change in the spatial distributions for the global pressure modes for different azimuthal and elevation angles; the dependence of the spatial distributions of the pressure POD modes are discussed in details in [14]. For each force component, there is a peak in spectra located between $0.1 < St < 0.2$, for both window geometries. It is especially pronounced in the y-component of the force, where a well-defined peak exists in this location. The magnitude of the peak is larger for the Az = 90 cases compared to the other azimuthal angles; it can be contributed to an dominant asymmetric pressure POD mode, see Figure 9, left plot; it was observed that the strength of this mode is increased when the smiles are located at Az = +-90 degree, as the smiles introduce additional surface discontinuities and, consequently, strong vortical structures with related pressure fluctuations into the flow downstream of smiles. This is the direct cause of the larger amplitude force in the y-direction for the Az = 90 cases.

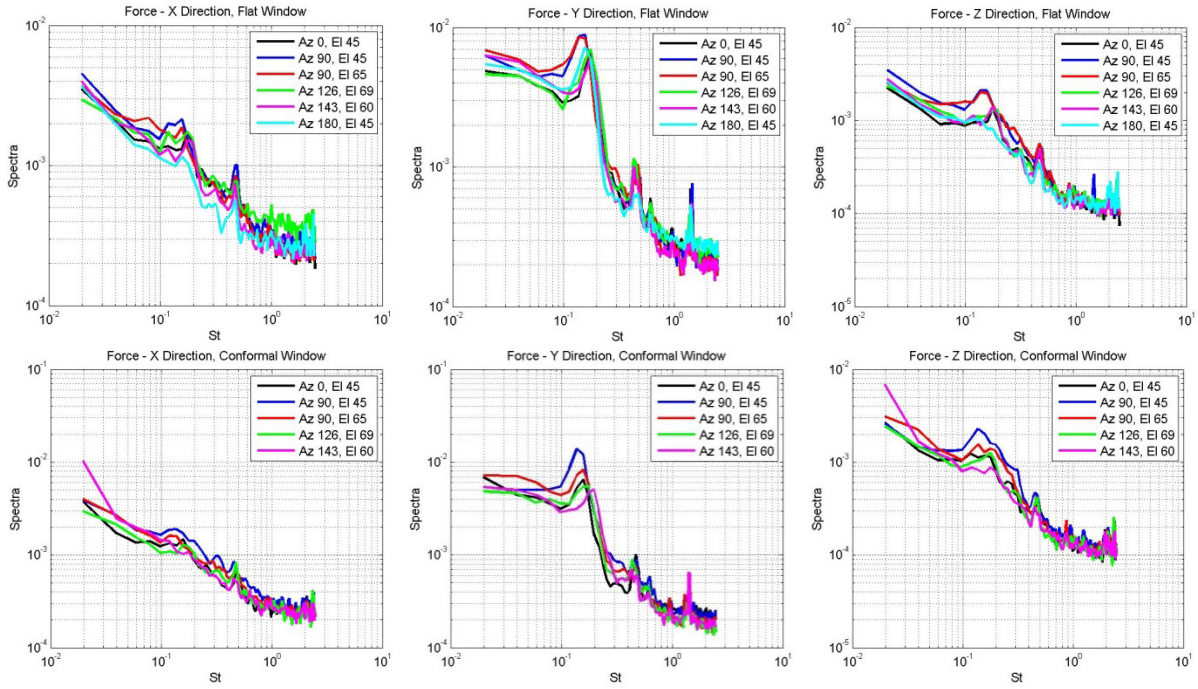

Figure 14. Forces from PSP tests, top – flat window, bottom - conformal window.

Figure 15 presents results of the in-flight force components estimated using the LSE-matrix from PSP-tests, but using the in-flight pressure data. They have very similar trends, as observed in force spectra computed from the tunnel experiments. There are no substantial magnitude differences between the force components, nor is there a substantial difference between the flat and conformal windows, in general. The only noticeable difference is that the peak at St = 0.2 for the y-component is much less pronounced. One possible explanation for these differences is that the tunnel measurements were performed at a lower M = 0.33, while flight data were collected at higher Mach numbers of 0.4 and 0.5, and some residual transition effects might still be present in pressure data at the lower Mach number. Similar transition-related Mach dependence was observed for aero-optical measurements at Mach numbers less than 0.35 [1]. More discussion of this effect will be provided in the next section.

There are a few other peaks missing from the force spectra approximated from flight, notably, a peak present between $0.4 < St < 0.5$ and a peak at St = 1.5, seen in the tunnel data in Figure 8. As these peaks are absent in all of the in-flight estimations, the nature of the tunnel-related peak are not quite clear, and possibly are induced by the tunnel fan. It should be emphasized that these flight-based force spectra are generated from a series of point measurements, and is possible that local phenomenon could impact the force substantially in a region not directly observed by a Kulite. This can be seen directly in the Az = 90°, El = 45° flat-window case. There are several peaks in the low-frequency region that are absent from the other cases.

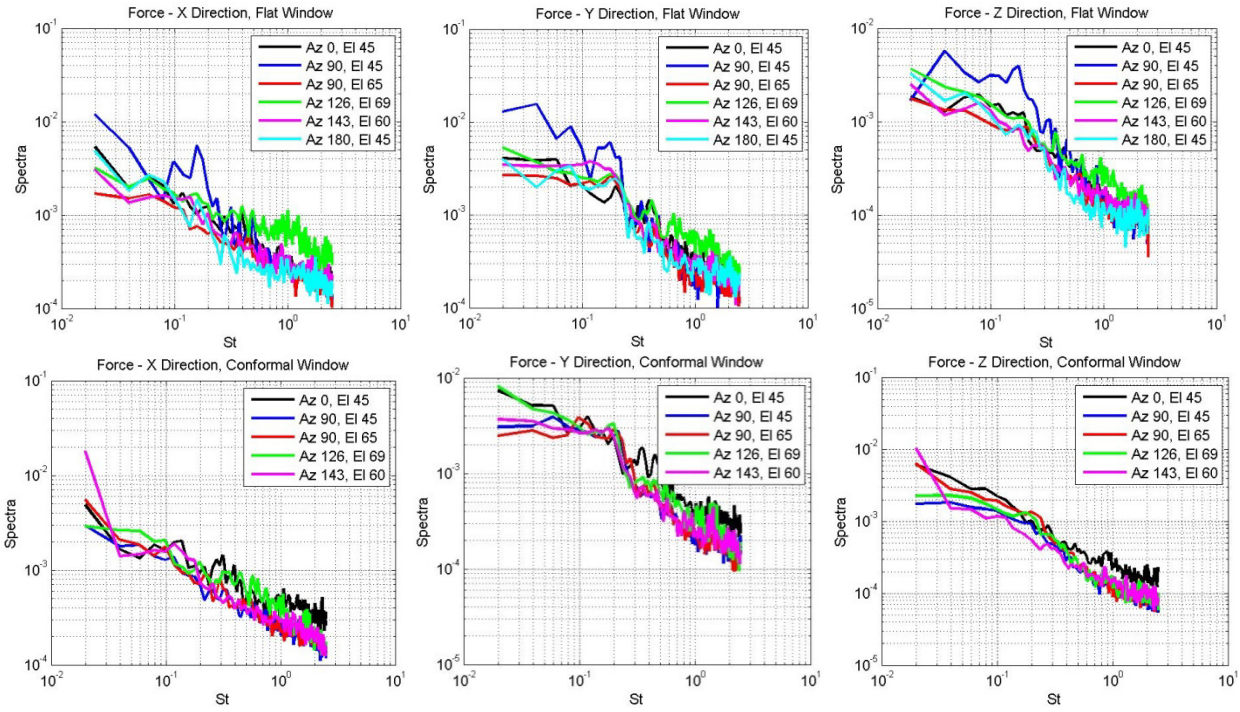

Figure 15. Forces approximated using flight data, top – flat window, bottom - conformal window.

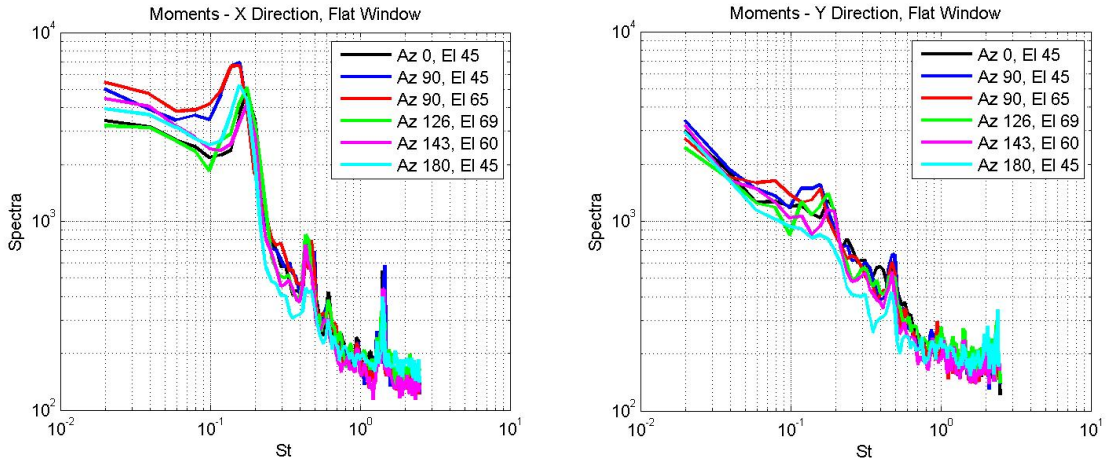

Figure 16. Moments about the center of the turret, in the x-y plane at the base of the turret in the z-plane integrated from PSP data, flat window.

In addition to forces, moments can also be integrated from the pressure field and estimated using the LSE-technique. The moments about the center of the turret, in the x-y plane at the base of the turret in the z-plane are given in Figure 16. The moment about the x-axis has the same peak between $0.1 < St < 0.2$ that was present in the y-direction forces. As with the forces, the moment magnitudes are very similar across the viewing angles, with the same increase in peak height in the x-axis moment for the Az = 90 cases. The two peaks that are suspected to be driven by the transition Mach number effects are also present in the integrated moments.

The time-averaged normalized RMS-values of all force components for all experimental cases are given in Table 3. As expected from the spectra analysis, RMS force values for the x and z directions are relatively consistent across all cases. The y-force components are largest for the Az = 90 cases, for the same rationale given previously. The flat window has a very limited effect on the RMS force values; as shown in the companion paper [14], global pressure modes are disrupted over the flat window, but this occurs over a small area relative to the area of the whole turret that the window geometry only minimally affects the unsteady forcing.

Table 3. Time-averaged normalized RMS Force values from PSP data.

Az	El	Window	F_{RMS} X	F_{RMS} Y	F_{RMS} Z
0	**45**	Flat	0.025	0.048	0.016
90	**45**	Flat	0.032	0.063	0.024
90	**65**	Flat	0.029	0.064	0.022
126	**69**	Flat	0.027	0.050	0.018
143	**60**	Flat	0.027	0.050	0.018
180	**45**	Flat	0.022	0.052	0.016
0	**45**	Conf.	0.031	0.053	0.022
90	**45**	Conf.	0.028	0.078	0.022
90	**65**	Conf.	0.028	0.064	0.022
126	**69**	Conf.	0.021	0.046	0.016

V. Flight/Tunnel Comparison

As shown previously, there are differences between the flight and tunnel force spectra, the most significant one is the peak found between $0.1 < St < 0.2$. It was mentioned previously and is shown in the companion paper [14] that the main driving mechanism for this peak is the dominant pressure mode on the turret, see Figures 7 and 9, left plots. To further investigate the effect of this pressure mode, forces and pressures at two different cases, Az = 90° and El = 65° with a conformal window and Az = 0° and El = 45° with a flat window, were examined at in more depth.

The force power spectra for the first of these cases are shown in Figure 17. The x- and z-force components match up fairly well between the flight and tunnel cases. The y-direction forces exhibit approximately the same shape between flight and tunnel testing, except below St = 0.2, where the in-flight amplitude is smaller. As discussed in Section 4.II, the y-force depends almost exclusively only on the first pressure POD mode. As discussed in details in [14], this dominant mode for this azimuthal angle is an anti-symmetric mode in the spanwise direction, implying the separations on both sides of the turret are correlated and out-of-phase. When the turret is at 90 degrees, the smiles are aligned in a cross-stream direction and, as the flow passes over the upstream smile edge, it becomes separated and vortical structures are formed along the sides of the turret. These structures, interacting with the separated region downstream of the turret, form a global correlation that appears to be the main driving force at this azimuthal angle. But due to the tunnel blockage and small Re-transition effects at lower speeds, the mode dynamics, which is directly related to the separation off the turret surface, might not be the same at M = 0.33, at which the tunnel data were collected and M = 0.5 for the in-flight data, possibly explaining a difference between y-force spectra observed in Figure 17, middle plot.

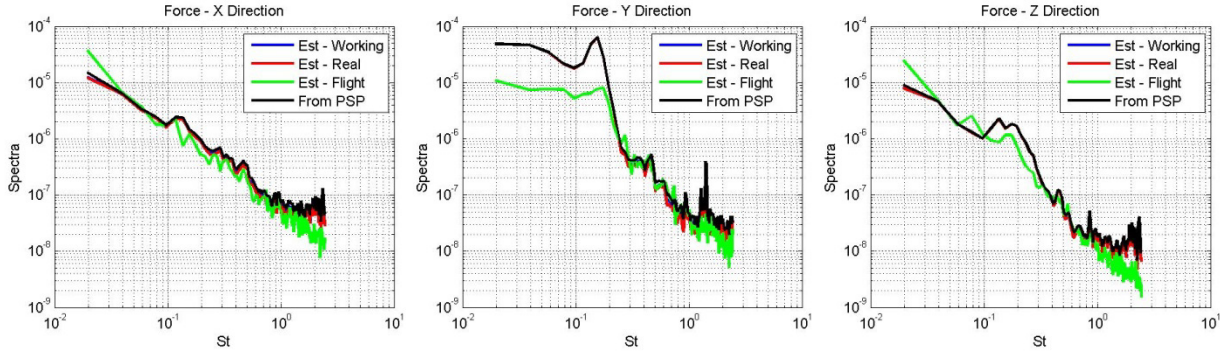

Figure 17. The spectra of the LSE-reconstruction of all components of the unsteady force using different number of in-flight pressure sensors compared the direct integration from PSP tests in the tunnel. The turret geometry was the conformal-window turret with Az = 90° and El = 65°.

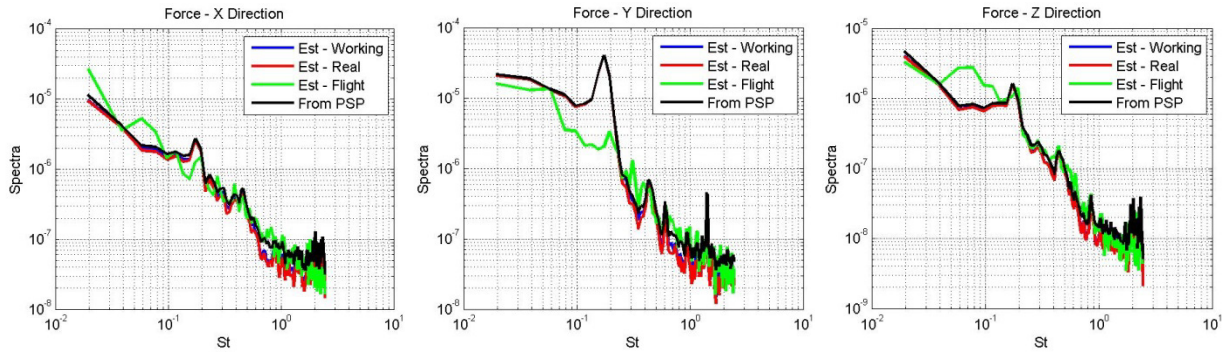

Figure 18. The spectra of the LSE-reconstruction of all components of the unsteady force using different number of in-flight pressure sensors compared with the direct integration from PSP tests in the tunnel. The turret geometry was the flat-window turret with Az = 0° and El = 45°.

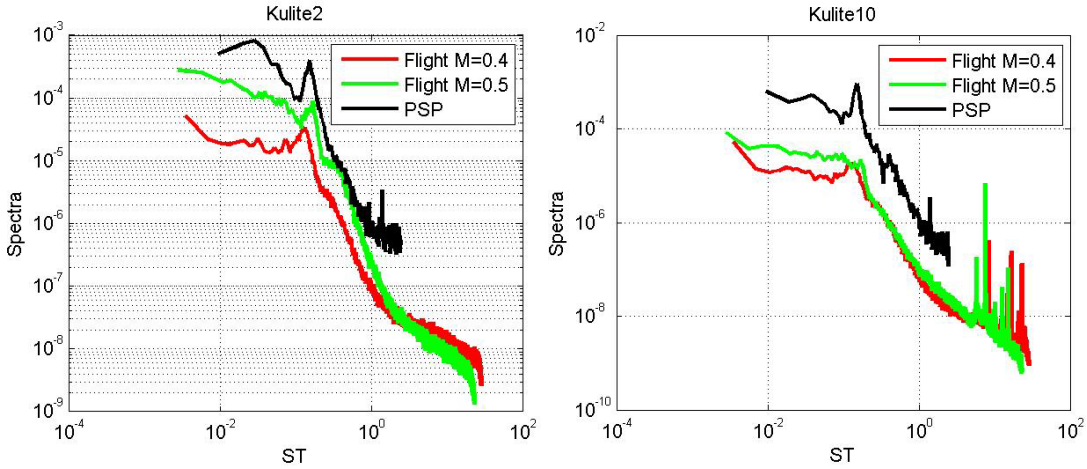

Figure 19. Pressure power spectra for two pressure sensors, K2 and K10, for the Az = 90°, El = 65° conformal window case. The two sensors are on opposite sides of the turret.

Comparison between the force spectra calculated directly from PSP tests in the tunnel and estimated from in-flight data for Az = 0° and El = 45° is presented in Figure 18. For this azimuthal angle, the smiles are located at the front and at the back of the turret and they do not cause any additional separations on either side of the turret. Overall shapes of the force spectra are generally the same, except for the peak at St = 0.15, which is reduced in magnitude for the y-force for the flight case. As the-y-force depends only on the first two POD modes, seen in Figure 8, this component is sensitive to the details of the flow separation and therefore likely to exhibit similar Re-transition behavior, as for Az = 90°. X- and z-forces depends on the first five POD modes, so the change in the first two modes affects them in lesser degree.

The same trends can be observed in the pressure spectra for kulites K2 and K10, which are on opposite sides of the turret. For the Az = 90°, El = 65° conformal window case, the spectra for these two kulites are shown in Figure 19. For this azimuthal angle the sensors are located near the separation region, where the dominant POD mode is essentially non-zero. For both of these locations, the PSP and in-flight kulite data at M = 0.5 both have a peak in the $0.1 < St < 0.2$ range; however, the peak has a substantially larger magnitude in the PSP cases, implying differences in the dynamics of the separation region between the tunnel and in-flight cases.

5. Conclusions

Two different experiments to characterize the unsteady pressure field on the surface of the hemisphere-on-cylinder turret were carried out. The first of these experiments used Pressure-Sensitive Paint to measure the full-surface, time-resolved surface pressure field for the turret in the Whitefield wind tunnel at M = 0.33. Local pressure measurements using eight unsteady pressure sensors were obtained simultaneously with the PSP to validate the PSP measurements. Additionally, the same turret was flown on the AAOL with a larger number (26) of unsteady

pressure sensors to obtain a series of local pressure measurements in-flight at speed of M = 0.5. Local surface temperatures were also obtained in both experiments.

One of the goals of these two experiments was to characterize an unsteady force applied to the turret, since the force ultimately is responsible for the aero-mechanical beam jitter that is observed in optical measurements. To accomplish this, the PSP-based pressures were integrated over the surface of the turret to obtain time histories of all three components of unsteady force and moments about the axes. These forcing values were then correlated with a series of point pressure measurements extracted with the PSP technique to create a response matrix that expresses each force and moment as a linear weighted summation of the local unsteady pressures. This was done in the frequency domain using the Linear Stochastic Estimation technique. After a proper normalization of all quantities by the dynamic pressure and the turret cross-sectional area, the response function can be used to approximate the unsteady forcing on turrets with different sizes, as long as they have the same geometry at the tested turret, at different flow conditions; the technique works under the assumption is that relevant pressure modes do not change spatial distribution at other speeds, but rather the amplitude only. Also, the influence of each of pressure modes, calculated using POD technique, on force components was also investigated.

From the response LSE-matrices, the integrated forces obtained from PSP tests and estimated from in-flight measurements were compared for several viewing angles for both a flat and conformal window turrets. The force spectra were similar between flight and tunnel testing except for a few distinct peaks, notably between $0.1 < St < 0.2$, where a peak was found in both the tunnel and flight y-component force spectra, but with a larger magnitude in the tunnel spectra. For both experiments, the peak was observed to have a larger magnitude with the turret at Az = 90°. This peak is related to the dominant, anti-symmetric pressure mode that acts primarily along the y-axis. At this azimuthal angle, the flow separates over the large surface slope discontinuities introduced by the smiles on both sides of the turret. This flow separation introduces additional vortical structures which, through non-linear interactions, lead to increase the magnitude of the dominant anti-symmetrical mode. In the tunnel, it is likely due to Re-transition effects and/or blockage there is an increase in the relative amplitude of this mode near St = 0.15. The characteristic peak in the spectrum of this mode appears in both the pressure spectra for in-flight kulites and tunnel PSP tests near the separation line on the turret, with a larger relative magnitude in the PSP spectra. Two other peaks at $0.4 < St < 0.5$ and St = 1.5 were observed only in the tunnel experiment. These two peaks are likely due to the tunnel fan.

The presented method of predicting in-flight unsteady forces using a sparse array of pressure sensors might be useful to estimate structural requirements for a turret mounting. The unsteady loading on the turret, combined with knowledge of the mounting structure can give an approximation of the aero-elastic turret response, as this response ultimately imposes a damaging aero-mechanical jitter introduced into the laser. Also, the information about the unsteady loading can be used to properly design a turret to minimize the mechanically-related beam jitter. Finally, knowledge of the unsteady forces acting to the turret and the overall unsteady pressure field can provide information about modified aero-dynamic properties of the aircraft that the turret is mounted in.

As the data from the third camera were found to be very noisy, thus limiting a present analysis to pressure field at the downstream half of the turret only, future work might involve performing additional PSP tests with different and more-sensitive cameras at higher Mach numbers, to avoid transition effects, to obtain the time-resolved pressure field over the entire surface of the turret. This would allow for the force approximation to account for any dominant pressure modes from the upstream portion of the turret. Additionally, if these unsteady pressure measurements are combined with simultaneous wavefront measurements over the turret aperture, it would provide very valuable information about the effect of the global flow topology around the turret on the local wavefront distortions.

6. Acknowledgments

This work was funded by the Air Force Research Laboratory, Directed Energy Directorate and the High Energy Laser Division of the Joint Technology Office (HEL JTO) and supported by the Air Force Office of Scientific Research through Grant number FA9550-07-1-0574. The U.S. Government is authorized to reproduce and distribute reprints for governmental purposes notwithstanding any copyright notation thereon.

The authors would like to thank the Northern Air personnel, especially Kevin Tessmer for providing technical assistance during flight tests. The authors also wish to thank Dr. Jim Crafton of Innovative Scientific Solutions, Inc. for his many useful suggestions about PSP measurements.

References

[1] S. Gordeyev and E. Jumper, “Fluid Dynamics and Aero-Optics of Turrets”, *Progress in Aerospace Sciences*, 46, (2010), pp. 388-400.

[2] N. De Lucca, S. Gordeyev and E.J. Jumper, **"**In-flight aero-optics of turrets", *Journal of Optical Engineering*, **52**(7), 071405, 2013.
[3] C. Porter, S.Gordeyev, M. Zenk and E. Jumper, "Flight Measurements of Aero-Optical Distortions from a Flat-Windowed Turret on the Airborne Aero-Optics Laboratory (AAOL)", AIAA Paper 2011-3280.
[4] M. Wang, A. Mani and S. Gordeyev, "Physics and Computation of Aero-Optics", *Annual Review of Fluid Mechanics*, Vol. **44**, pp. 299-321, 2012.
[5] P.E. Morgan and M.R. Visbal., "Hybrid Reynolds-Averaged Navier-Stokes/Large-Eddy Simulation Investigating Control of Flow over a Turret", *Journal of Aircraft*, **49**(*6*), pp. 1700-1717, 2012.
[6] R. Jelic, S. Sherer and R.Greendyke, "Simulation of Various Turret Configurations at Subsonic and Transonic Flight Conditions Using OVERFLOW", AIAA Paper 2012-464, 2012.
[7] B. Vukasinovic, A. Glezer, S Gordeyev and E. Jumper, "Flow Control for Aero-Optics Application", *Experiments in Fluids*, **54**, p. 1492, 2013.
[8] S. Gordeyev, J.A. Cress, E. Jumper and A.B. Cain, "Aero-Optical Environment Around a Cylindrical Turret with a Flat Window", *AIAA Journal*, Vol. 49, No. 2, pp. 308-315, 2011.
[9] N. De Lucca, S. Gordeyev and E. Jumper, "The Study of Aero-Optical and Mechanical Jitter for Flat Window Turrets", AIAA Paper 2012-0623.
[10] E.J. Jumper, M. Zenk, S. Gordeyev, D. Cavalieri and M.R. Whiteley, "Airborne Aero-Optics Laboratory", *Journal of Optical Engineering*, **52**(7), 071408, 2013.
[11] K. Hird, T. J. Juliano, J, Gregory, N. Delucca, S. Gordeyev, E. Jumper, J. Thordahl and D.J. Wittich, "Study of Unsteady Surface Pressure on a Turret via Pressure-Sensitive Paint", to be presented at 43rd AIAA Fluid Dynamics Conference, San Diego, CA, 24-27 June 2013.
[12] Gregory, J. W., Asai, K., Kameda, M., Liu, T., and Sullivan, J. P., "A Review of Pressure-Sensitive Paint for High-Speed and Unsteady Aerodynamics," *Proceedings of the Institution of Mechanical Engineers, Part G: Journal of Aerospace Engineering,* Vol. **222**, No. 2, 2008, pp. 249-290.
[13] Tan, T.N., Sullivan, G.D., and Baker, K.D. 1993. On computing the perspective transformation matrix and camera parameters. In Proc. of 4th British Machine Vision Conf., Surrey, England, pp. 125–134.
[14] S. Gordeyev, N. Delucca, E. Jumper, K. Hird, T. J. Juliano, J, Gregory, J. Thordahl and D.J. Wittich, "The Comparison of Unsteady Pressure Field over Flat- and Conformal-Window Turrets using Pressure Sensitive Paint", to be presented at 43rd AIAA Fluid Dynamics Conference, San Diego, CA, 24-27 June 2013.
[15] Adrian, R.J., "On the role of conditional averages in turbulent theory", In: Turbulence in Liquids: Proceedings of the 4th Biennial Symposium on Turbulence in Liquids, ed. G. Patteson and J. Zakin, Science Press, Princeton, 1977, pp. 322-33.
[16] G. Berkooz, P. Holmes, and J. Lumley, "The Proper Orthogonal Decomposition in the Analysis of Turbulent Flows", *Annual Review of Fluid Mechanics*, Vol. 25, No. 1, pp. 539-575, 1993.